

Cavitation in a quark gluon plasma with finite chemical potential and several transport coefficients

S. M. Sanches Jr.†, D. A. Fogaça†, F. S. Navarra† and H. Marrochio†

† *Instituto de Física, Universidade de São Paulo*

Rua do Matão Travessa R, 187, 05508-090, São Paulo, SP, Brazil

Abstract

We study the effects of a finite chemical potential on the occurrence of cavitation in a quark gluon plasma (QGP). We solve the evolution equations of second order viscous relativistic hydrodynamics using three different equations of state. The first one was derived in lattice QCD and represents QGP at zero chemical potential. It was previously used in the study of cavitation. The second equation of state also comes from lattice QCD and is a recent parametrization of the QGP at finite chemical potential. The third one is similar to the MIT equation of state with chemical potential and includes nonperturbative effects through the gluon condensates. We conclude that at finite chemical potential cavitation in the QGP occurs earlier than at zero chemical potential. We also consider transport coefficients from a holographic model of a non-conformal QGP at zero chemical potential. In this case cavitation does not occur.

I. INTRODUCTION

The analysis of an extensive body of experimental information suggests that in the heavy ion collisions at high energies performed at the Relativistic Heavy Ion Collider (RHIC) [1, 2] and the Large Hadron Collider (LHC) [3] a quark gluon plasma (QGP) is formed and it behaves like an almost perfect fluid [4]. This highly energetic fluid is very well described by relativistic hydrodynamics [5–8]. In ordinary fluids such as water, the effective pressure can be different from the equilibrium pressure and, in particular, in some situations it can drop below the vapor pressure. In this case, the thermodynamically preferred phase becomes the gaseous, and a vapor bubble forms inside the fluid, a phenomenon known as cavitation. In the case of relativistic fluids such as the QGP studied in heavy-ion collisions, cavitation would imply a phase transition from a deconfined plasma phase of quarks and gluons to a confined hadron-gas phase. The resulting medium would be highly inhomogeneous with (possibly short-lived) hadron gas bubbles expanding and collapsing in an otherwise laminar fluid. The study of cavitation in the QGP was pioneered by the authors of Refs. [9, 10] and further developed in Ref. [11].

In the present work we extend the formalism employed in [11] to the case of finite chemical potential. From phenomenological studies of particle production in heavy ion collisions with the help of thermal models [12] we can conclude that the baryon chemical potential is of the order of $\mu_B \simeq 1 - 10$ MeV at LHC and $\mu_B \simeq 20 - 100$ MeV at RHIC. At lower energies, the chemical potential can reach higher values, $\mu_B \simeq 500$ MeV. Moreover, in the case of inhomogeneous freeze-out, even at high energies we can have domains of high chemical potential [13]. Recently the equation of state (EOS) of the QGP at finite chemical potential was computed in lattice QCD simulations [14, 15]. In view of these results, we think that it is interesting to investigate the effect of finite chemical potential on cavitation. In the search for different phenomenological parametrizations of the bulk viscosity coefficient and other transport parameters, based on different many-body microscopic dynamics, we have considered the holographic non-conformal model of QGP of Ref. [16].

II. SECOND ORDER RELATIVISTIC VISCOUS HYDRODYNAMICS

A. The main equations

Throughout this study we use natural units $\hbar = c = k_B = 1$. The energy momentum tensor of viscous relativistic hydrodynamics [11, 16–19] is:

$$T^{\mu\nu} = \varepsilon u^\mu u^\nu - p \Delta^{\mu\nu} + \Pi^{\mu\nu} \quad (1)$$

where the ε and p are the energy density and the pressure of the fluid, $u^\mu = (\gamma, \gamma \vec{v})$ is the 4-velocity of the fluid (γ is the Lorentz factor $\gamma = (1 - v^2)^{-1/2}$) with normalization $u_\mu u^\mu = -1$. The metric is given by $g_{\mu\nu} = \text{diag}(-, +, +, +)$. $\Pi^{\mu\nu}$ is the viscous tensor satisfying $u_\mu \Pi^{\mu\nu} = 0$ and $\Delta^{\mu\nu} \equiv g^{\mu\nu} + u^\mu u^\nu$ is the projector orthogonal to u^μ . Notice that we do not include dissipative currents associated with finite chemical potential and heat flow. In Bjorken flow [21], symmetry constraints eliminate these contributions from the equations of motion [22].

Conservation of the energy and momentum is enforced by $\nabla_\mu T^{\mu\nu} = 0$, where ∇_μ is the covariant derivative. The projection of this equation on the direction parallel to the fluid velocity reads: $u_\nu \nabla_\mu T^{\mu\nu} = 0$. Similarly, the projection on the direction perpendicular to the fluid velocity yields: $\Delta_\nu^\alpha \nabla_\mu T^{\mu\nu} = 0$. These two projections lead to the following evolution equations [11, 16, 19]:

$$D\varepsilon + (\varepsilon + p)\theta + \Pi^{\mu\nu} \nabla_\perp{}_{(\mu} u_{\nu)} = 0 \quad (2)$$

and

$$(\varepsilon + p)Du^\mu + \nabla_\perp{}^\mu p + \Delta_\alpha^\mu \nabla_\beta \Pi^{\alpha\beta} = 0 \quad (3)$$

In the above equations we have $D \equiv u^\mu \nabla_\mu$, $\theta \equiv \nabla_\mu u^\mu$, $\nabla_\perp{}^\mu \equiv \Delta^{\mu\alpha} \nabla_\alpha$ and the symmetrization of the indices is represented by $A_{(\mu\nu)} = (A_{\mu\nu} + A_{\nu\mu})/2$.

The viscous tensor $\Pi^{\mu\nu}$ is given by [11, 16, 17]:

$$\Pi^{\mu\nu} = \pi^{\mu\nu} + \Pi \Delta^{\mu\nu} \quad (4)$$

where $\pi^{\mu\nu}$ is the traceless symmetric part $\pi^\nu{}_\nu = 0$ and $\Pi \equiv g_{\mu\nu} \Pi^{\mu\nu}/3$. We obtain the components of the viscous tensor (4) solving the following equations [11, 16, 19] which are second order Israel-Stewart like [20]:

$$\tau_\Pi^\eta \left(D\pi^{\langle\mu\nu\rangle} + \frac{4}{3}\theta\pi^{\mu\nu} \right) + \pi^{\mu\nu} = -2\eta\sigma^{\mu\nu} + \frac{\lambda_1}{\eta^2} \pi_\lambda^{\langle\mu} \pi^{\nu\rangle\lambda} \quad (5)$$

$$\Pi = -\zeta\theta - \tau_{\text{II}}^{\zeta} D\Pi \quad (6)$$

with the definitions $\sigma^{\mu\nu} \equiv \Delta^{\mu\nu\alpha\beta} \nabla_{\alpha} u_{\beta}$, $\Delta^{\mu\nu\alpha\beta} \equiv (\Delta^{\mu\alpha} \Delta^{\nu\beta} + \Delta^{\mu\beta} \Delta^{\nu\alpha})/2 - \Delta^{\mu\nu} \Delta^{\alpha\beta}/3$ and $A^{(\mu\nu)} \equiv \Delta^{\mu\nu\alpha\beta} A_{\alpha\beta}$.

The shear viscosity is η , and the second-order coefficients are τ_{II}^{η} and λ_1 , given by the holographic calculations of $\mathcal{N} = 4$ SYM [23, 24]:

$$\frac{\eta}{s} = \frac{1}{4\pi} \quad (7)$$

$$\tau_{\text{II}}^{\eta} = \frac{[2 - \ln(2)]}{2\pi T} \quad (8)$$

$$\lambda_1 = \frac{\eta}{2\pi T} = \frac{s}{8\pi^2 T} \quad (9)$$

and by the following parametrization of ζ/s [11, 18]:

$$\frac{\zeta}{s} = a \exp\left(\frac{T_c - T}{\Delta T}\right) + b \left(\frac{T_c}{T}\right)^2 \quad \text{for } T > T_c \quad (10)$$

whith $a = 0.901$, $b = 0.061$ and $\Delta T = T_c/14.5$. We also consider $\tau_{\text{II}}^{\eta} = \tau_{\text{II}}^{\zeta}$. We obtain the entropy density from the relation

$$s = \frac{\partial p}{\partial T} \quad (11)$$

For this parametrization we will choose $T_c = 190 \sim 200 \text{ MeV}$. Setting the second-order coefficients equal to zero ($\tau_{\text{II}}^{\eta} = 0$, $\tau_{\text{II}}^{\zeta} = 0$ and $\lambda_1 = 0$) we recover the Navier-Stokes approach in (5) and (6): $\pi^{\mu\nu} = -2\eta\sigma^{\mu\nu}$ and $\Pi = -\zeta\theta$.

B. Bjorken flow

Now we consider solutions of the hydrodynamical equations which do not depend on the transverse spatial coordinates x and y and are boost invariant in the z -direction as in [11, 16, 18], which are the Bjorken symmetries. To obtain the evolution equations in this boost invariant description we perform the changes of variables from (t, z) to (τ, ξ) , where τ is the proper time and ξ is the spacetime rapidity, given by [21]: $\tau \equiv \sqrt{t^2 - z^2}$ and $\xi \equiv \tanh^{-1}(z/t)$. In general, the Milne coordinates are (τ, r, ϕ, ξ) and the line element is $ds^2 = -d\tau^2 + dr^2 + r^2 d\phi^2 + \tau^2 d\xi^2$ so $g_{\mu\nu} = \text{diag}(-1, 1, 1, \tau^2)$. Due to the Bjorken symmetry the four-velocity in Milne coordinates turns out to be $u^{\mu} = (1, 0, 0, 0)$.

In the (τ, ξ) coordinates we have $\theta = 1/\tau$, $D = \nabla_\tau$, $\Gamma_{\tau\xi}^\xi = \Gamma_{\xi\tau}^\xi = 1/\tau$, $\Gamma_{\xi\xi}^\tau = \tau$ and $\nabla_\mu u_\nu = -\Gamma_{\mu\nu}^\lambda u_\lambda = \Gamma_{\mu\nu}^\tau$. In particular, $\nabla_\xi u_\xi = \tau$.

The energy-momentum tensor (1) becomes:

$$T_\nu^\mu = \begin{pmatrix} \varepsilon & 0 & 0 & 0 \\ 0 & p & 0 & 0 \\ 0 & 0 & p & 0 \\ 0 & 0 & 0 & p \end{pmatrix} + \begin{pmatrix} 0 & 0 & 0 & 0 \\ 0 & \Pi + \frac{\Phi}{2} & 0 & 0 \\ 0 & 0 & \Pi + \frac{\Phi}{2} & 0 \\ 0 & 0 & 0 & \Pi - \Phi \end{pmatrix} \quad (12)$$

where the contributions to the pressure from the bulk and shear stresses are respectively given by Π (the trace of $\Pi^{\alpha\beta}$) and Φ (the traceless part of $\Pi^{\alpha\beta}$), given by $\pi_x^x = \pi_y^y \equiv \Phi/2$ and $\pi_\xi^\xi = -\Phi$.

From (12) we identify the transverse pressure:

$$P_\perp \equiv p + \Pi + \frac{\Phi}{2} \quad (13)$$

and the longitudinal pressure:

$$P_\xi \equiv p + \Pi - \Phi \quad (14)$$

In the (τ, ξ) description, the equations (2), (3) and (4) give the following evolution equations [11]:

$$\frac{\partial \varepsilon}{\partial \tau} = -\frac{\varepsilon + p + \Pi - \Phi}{\tau} \quad (15)$$

$$\tau_\Pi^\eta \frac{\partial \Phi}{\partial \tau} = \frac{4\eta}{3\tau} - \Phi - \left[\frac{4\tau_\Pi^\eta}{3\tau} \Phi + \frac{\lambda_1}{2\eta^2} \Phi^2 \right] \quad (16)$$

and

$$\tau_\Pi^\zeta \frac{\partial \Pi}{\partial \tau} = -\frac{\zeta}{\tau} - \Pi. \quad (17)$$

Cavitation will take place when the longitudinal pressure P_ξ becomes negative.

III. EQUATION OF STATE

In this work we study the occurrence of cavitation considering three equations of state for the quark gluon plasma.

A. Model 1

The following EOS was previously employed in [11] and we use it to perform comparison with other models. This equation of state describes the quark gluon plasma phase and the crossover to a hadron gas, being a parametrization of a lattice calculation at zero chemical potential with $T_c = 190 \text{ MeV}$. The trace anomaly is given by [25]:

$$\frac{\varepsilon_1 - 3p_1}{T^4} = \left(1 - \frac{1}{\left[1 + \exp\left(\frac{T-c_1}{c_2}\right) \right]^2} \right) \left(\frac{d_2}{T^2} + \frac{d_4}{T^4} \right) \quad (18)$$

$d_2 = 0.24 \text{ GeV}^2$, $d_4 = 0.0054 \text{ GeV}^4$, $c_1 = 0.2073 \text{ GeV}$ and $c_2 = 0.0172 \text{ GeV}$. The pressure [11] is:

$$p_1 = T^4 \int_{T_0}^T dT' \left(1 - \frac{1}{\left[1 + \exp\left(\frac{T'-c_1}{c_2}\right) \right]^2} \right) \left(\frac{d_2}{T'^3} + \frac{d_4}{T'^5} \right) \quad (19)$$

From (18) and (19) we obtain the energy density:

$$\begin{aligned} \varepsilon_1 &= T^4 \left(1 - \frac{1}{\left[1 + \exp\left(\frac{T-c_1}{c_2}\right) \right]^2} \right) \left(\frac{d_2}{T^2} + \frac{d_4}{T^4} \right) \\ &+ 3T^4 \int_{T_0}^T dT' \left(1 - \frac{1}{\left[1 + \exp\left(\frac{T'-c_1}{c_2}\right) \right]^2} \right) \left(\frac{d_2}{T'^3} + \frac{d_4}{T'^5} \right) \end{aligned} \quad (20)$$

B. Model 2

In this work we study finite chemical potential effects in cavitation. To do so, we use the recent parametrization of a lattice simulation of $SU(3)$ QCD matter at finite temperature and chemical potential, with quarks (u , d and s with equal masses) and gluons [14, 15].

We have previously used this equation of state in the study of the expansion of the early Universe in [26], where we have developed the expressions in detail. We start by recalling the trace anomaly at finite chemical potential [14, 15]:

$$\begin{aligned} \frac{\varepsilon_2(T, \mu) - 3p_2(T, \mu)}{T^4} &= T \frac{\partial}{\partial T} \left[\frac{p_2(T, \mu)}{T^4} \right] + \frac{\mu^2}{T^2} \chi_2 \\ &= \frac{\varepsilon_2(T, 0) - 3p_2(T, 0)}{T^4} + \frac{\mu^2}{2T} \frac{d\chi_2}{dT} \end{aligned} \quad (21)$$

where the chemical potential contribution is given by the function [14]:

$$\chi_2(T) = e^{-h_3/\tau - h_4/\tau^2} \cdot f_3 \cdot \left[\tanh(f_4 \cdot \tau + f_5) + 1 \right] \quad (22)$$

In the zero chemical potential limit we have [14, 15]:

$$\frac{\varepsilon_2(T, 0) - 3p_2(T, 0)}{T^4} = e^{-h_1/\tau - h_2/\tau^2} \cdot \left[h_0 + \frac{f_0 \cdot \left[\tanh(f_1 \cdot \tau + f_2) + 1 \right]}{1 + g_1 \cdot \tau + g_2 \cdot \tau^2} \right]. \quad (23)$$

In the last three expressions we have introduced the variable $\tau = T/200 \text{ MeV}$, where 200 MeV is the critical temperature. For the dimensionless parameters we take [15]: $h_0 = 0.1396$, $h_1 = -0.1800$, $h_2 = 0.0350$, $f_0 = 1.05$, $f_1 = 6.39$, $f_2 = -4.72$, $g_1 = -0.92$ and $g_2 = 0.57$. From [14] we have $h_3 = -0.5022$, $h_4 = 0.5950$, $f_3 = 0.1359$, $f_4 = 6.3290$ and $f_5 = -4.8303$. The pressure is calculated from (21):

$$p_2(T, \mu) = T^4 \int_0^T dT' \frac{e^{-h_1/\tau' - h_2/\tau'^2}}{T'} \cdot \left[h_0 + \frac{f_0 \cdot \left[\tanh(f_1 \cdot \tau' + f_2) + 1 \right]}{1 + g_1 \cdot \tau' + g_2 \cdot \tau'^2} \right] + \frac{\chi_2}{2} \mu^2 T^2 \quad (24)$$

Inserting (24) into (21) we find the following expression for the energy density [26]:

$$\begin{aligned} \varepsilon_2(T, \mu) &= T^4 e^{-h_1/\tau - h_2/\tau^2} \cdot \left[h_0 + \frac{f_0 \cdot \left[\tanh(f_1 \cdot \tau + f_2) + 1 \right]}{1 + g_1 \cdot \tau + g_2 \cdot \tau^2} \right] + \frac{\mu^2}{2} T^3 \frac{d\chi_2}{dT} \\ &+ 3T^4 \int_0^T dT' \frac{e^{-h_1/\tau' - h_2/\tau'^2}}{T'} \cdot \left[h_0 + \frac{f_0 \cdot \left[\tanh(f_1 \cdot \tau' + f_2) + 1 \right]}{1 + g_1 \cdot \tau' + g_2 \cdot \tau'^2} \right] + \frac{3\chi_2}{2} \mu^2 T^2 \end{aligned} \quad (25)$$

C. Model 3

The equation of state considered in this subsection is obtained with the finite temperature mean field theory approach to QCD and includes three quark flavors with equal masses and gluons. This EOS is an improvement of the previous works [26–28]. We use the effective Lagrangian derived in [27] in the finite temperature formalism developed in [29]. The pressure is given by:

$$p_3 = \frac{3g^2}{16m_g^2} \rho^2 - \mathcal{B}_{QCD} + \sum_{f=u}^{d,s} \frac{\gamma_f}{6\pi^2} \int_0^\infty dk \frac{k^4}{\sqrt{m_f^2 + k^2}} \left(d_f + \bar{d}_f \right) + \frac{\gamma_g}{6\pi^2} \int_0^\infty dk k^2 \left(e^{k/T} - 1 \right)^{-1} \quad (26)$$

and the energy density reads [26]

$$\varepsilon_3 = \frac{3g^2}{16m_g^2}\rho^2 + \mathcal{B}_{QCD} + \sum_{f=u}^{d,s} \frac{\gamma_f}{2\pi^2} \int_0^\infty dk k^2 \sqrt{m_f^2 + k^2} (d_f + \bar{d}_f) + \frac{\gamma_g}{2\pi^2} \int_0^\infty dk k^2 (e^{k/T} - 1)^{-1} \quad (27)$$

where the Fermi distribution functions are

$$d_f \equiv \frac{1}{1 + e^{(\mathcal{E}_f - \nu_f)/T}} \quad \text{and} \quad \bar{d}_f \equiv \frac{1}{1 + e^{(\mathcal{E}_f + \nu_f)/T}} \quad (28)$$

The energy of the quark of flavor f is given by $\mathcal{E}_f = \sqrt{m_f^2 + k^2}$ and ν_f is the corresponding chemical potential. The quark density is given by:

$$\rho = \sum_{f=u}^{d,s} \frac{\gamma_f}{2\pi^2} \int_0^\infty dk k^2 (d_f - \bar{d}_f) \quad (29)$$

The statistical factors are given by $\gamma_g = 2(\text{polarizations}) \times 8(\text{colors}) = 16$ for gluons and $\gamma_f = 2(\text{spins}) \times 3(\text{colors}) = 6$ for each quark species, and $\mu \equiv \nu_u = \nu_d = \nu_s$ is the common chemical potential for the quarks. Setting $g = 0$ we recover the equation of state of the bag model at finite chemical potential. Setting $g = 0$ and also $\mu = 0$ we recover the usual bag model equation of state [21, 31]. As in [26], for example, we fix the coupling constant at $g = 0.6$ and the dynamical gluon mass at $m_g = 200 \text{ MeV}$. We will choose the bag constant \mathcal{B}_{QCD} in the interval $50 \leq \mathcal{B}_{QCD} \leq 150 \text{ MeV}/fm^3$. The term proportional to $(g/m_g)^2$ [26–28] in (26) and (27) may enhance the chemical potential effects. Such term does not exist in the usual bag model [21, 31, 32].

D. Numerical Results

We start our numerical study following the calculations developed in [11], with no bulk effects and considering that the evolution starts at $\tau_0 = 0.5 fm$, with $\Phi(\tau_0) = 0$. We want to compare different equations of state and determine the effects of certain features of these EOS (such as, for example, finite chemical potential) on the evolution of the fluid. To do this we would like to evolve them starting from the same initial state. However this is not possible because if they represent systems at the same initial temperature, then, these systems will have different initial energy densities and vice-versa. In relativistic heavy ion collisions, before thermal equilibrium formation, energy is released from the projectiles in

a certain volume in the central rapidity region. It is perhaps more realistic to say that the quark-gluon system has first a defined energy density determined from the conditions of the collisions and then it reaches thermal equilibrium, forming a QGP with the properties determined by the equation of state. Since it is very difficult to know what comes first, energy density or temperature, we will test the two possibilities: same initial temperature, $T_{initial} = 305 \text{ MeV}$ and same initial energy density, $\varepsilon_{initial} = 16 \text{ GeV}/fm^3$. We will find out that our conclusions regarding cavitation do not depend on this choice and are the same for different initial conditions.

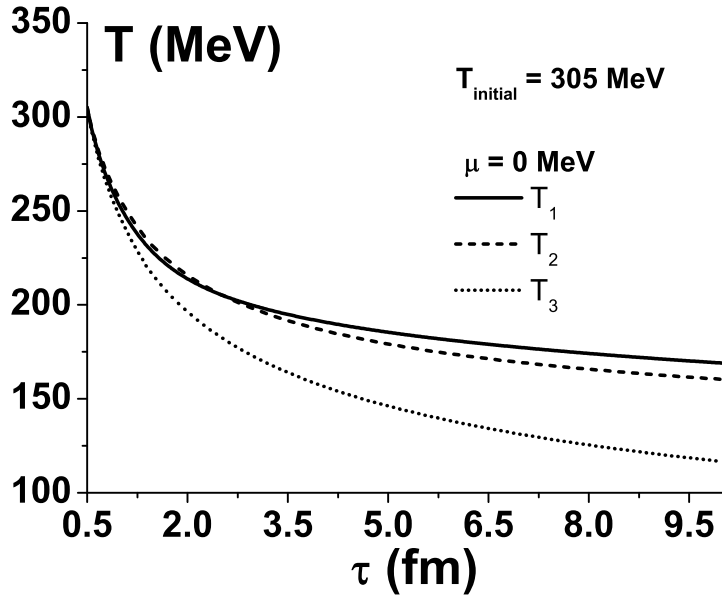
We solve the coupled equations (15) and (16) to obtain the temperature for each model considered. The temperature evolution at zero chemical potential is showed in Fig. 1. The effects of the chemical potential are presented in Fig. 2 for *Model 2* and *Model 3*. From the figure we clearly see that systems with larger chemical potential cool faster.

Cavitation is an effect mostly associated with peaks of the bulk viscosity close to phase transition [11, 17, 18]. We now consider bulk effects via eq. (17) with the relaxation scale approximated by $\tau_{\Pi}^{\eta} = \tau_{\Pi}^{\zeta}$. As previously mentioned, cavitation is generated when the longitudinal pressure, P_{ξ} , is negative and it starts when $P_{\xi}(\tau_{cav}) = 0$ in (14), where τ_{cav} is the time at which the longitudinal pressure vanishes. In this subsection we will make use of (7) to (11) to solve numerically the three coupled evolution equations (15), (16) and (17) and determine the time evolution of the longitudinal pressure (14).

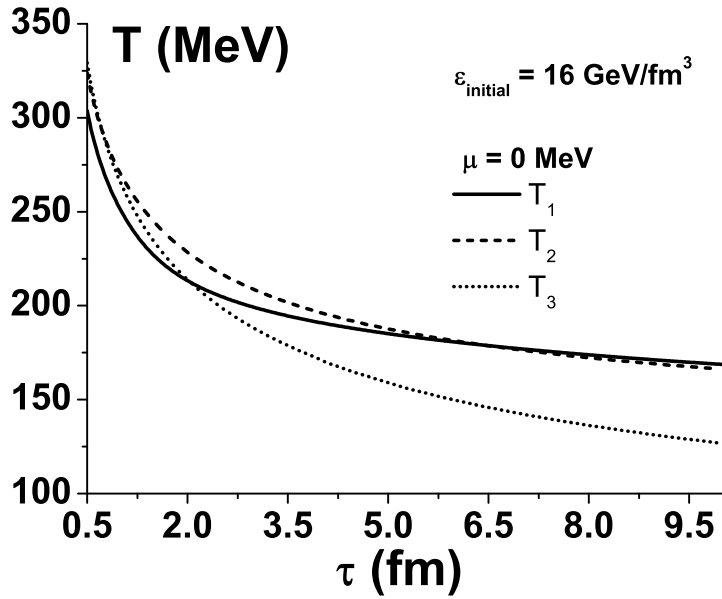
We start with zero chemical potential in Fig. 3 for the three models with the initial conditions $\tau_0 = 0.5 \text{ fm}$, $\Phi(\tau_0) = 0$, $\Pi(\tau_0) = 0$ for $T_{initial} = 305 \text{ MeV}$ and also for $\varepsilon_{initial} = 16 \text{ GeV}/fm^3$. For comparison we show *Model 3* for two bag constants: $\mathcal{B}_{QCD} = 50 \text{ MeV}/fm^3$ and $\mathcal{B}_{QCD} = 150 \text{ MeV}/fm^3$, and we conclude that increasing the bag value cavitation occurs earlier.

TABLE I: Time when cavitation starts (in Fig. 3(a))

$\tau_{cav} \text{ [fm]} \quad (\text{fixed } T_{initial} = 305 \text{ MeV})$	
<i>Model 1</i>	2.3
<i>Model 2</i>	2.9
<i>Model 3</i> ($\mathcal{B}_{QCD} = 50 \frac{\text{MeV}}{fm^3}$)	1.71
<i>Model 3</i> ($\mathcal{B}_{QCD} = 150 \frac{\text{MeV}}{fm^3}$)	1.61

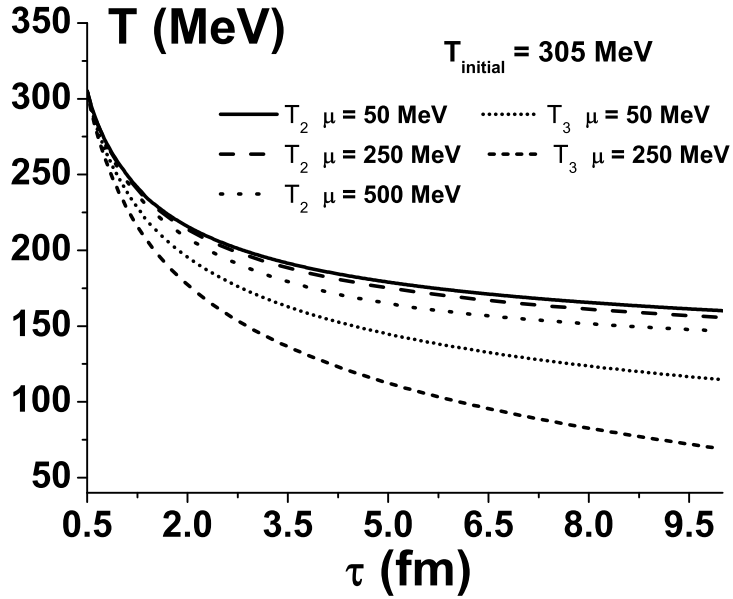


(a)

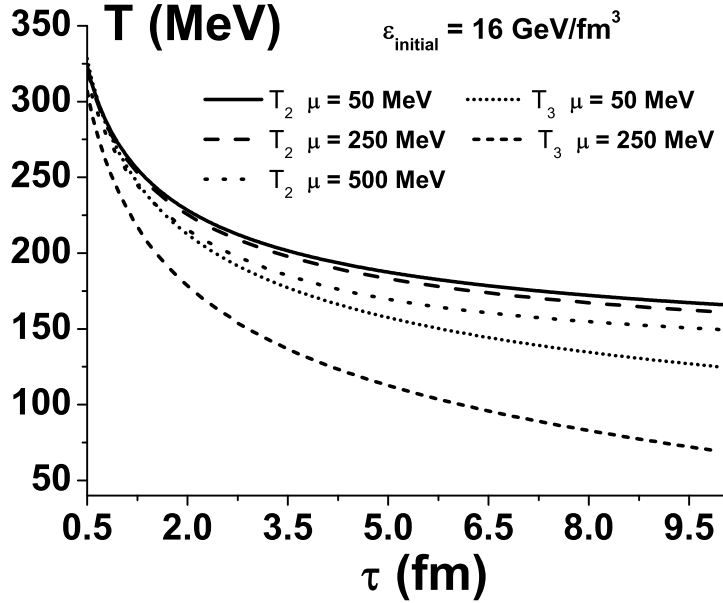


(b)

FIG. 1: Temperature evolution with no bulk effects for the three models from $\tau_0 = 0.5 \text{ fm}$ to $\tau_{\text{final}} = 10 \text{ fm}$ at zero chemical potential. The results for the *Model 3* were obtained with $\mathcal{B}_{QCD} = 150 \text{ MeV/fm}^3$. a) Same initial temperature. b) Same initial energy density.

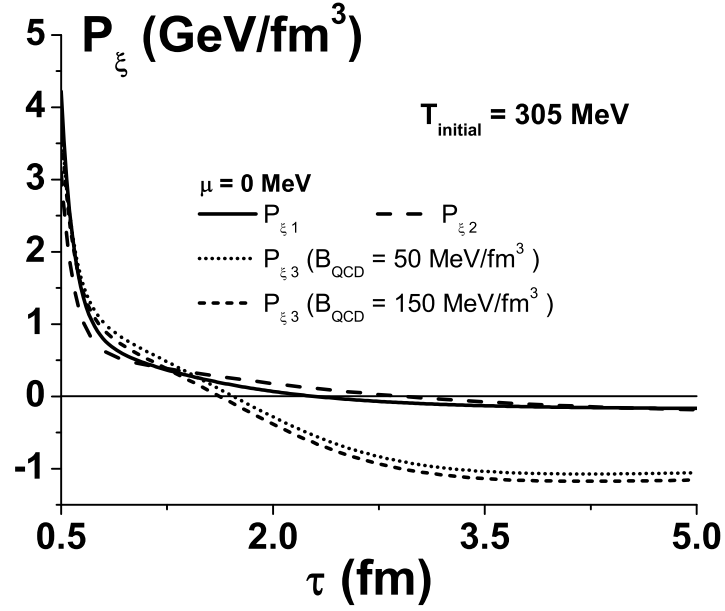


(a)

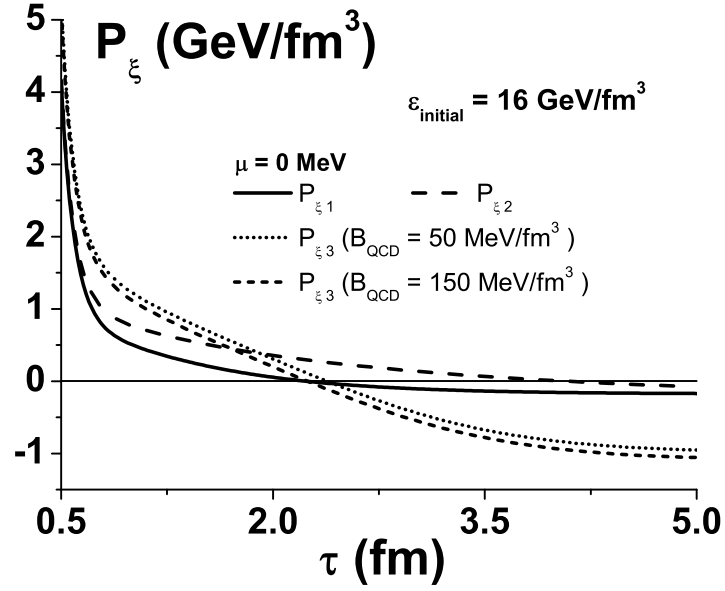


(b)

FIG. 2: Temperature evolution with no bulk effects for *Model 2* and *Model 3* from $\tau_0 = 0.5$ fm to $\tau_{\text{final}} = 10$ fm at finite chemical potential. For the *Model 3* we set $B_{QCD} = 150$ MeV/fm³, $g = 0.6$ and $m_g = 200$ MeV. a) Same initial temperature. b) Same initial energy density.



(a)



(b)

FIG. 3: Time evolution of the longitudinal pressure (14) from $\tau_0 = 0.5 \text{ fm}$ and zero chemical potential. See Tables I and II. a) Same initial temperature. b) Same initial energy density.

In Fig. 4 we show results at finite chemical potentials for *Models 2* and *3*. In both models

TABLE II: Time when cavitation starts (in Fig. 3(b))

$\tau_{cav} [fm]$ (fixed $\varepsilon_{initial} = 16 GeV/fm^3$)	
<i>Model 1</i>	2.22
<i>Model 2</i>	4.06
<i>Model 3</i> ($\mathcal{B}_{QCD} = 50 \frac{MeV}{fm^3}$)	2.38
<i>Model 3</i> ($\mathcal{B}_{QCD} = 150 \frac{MeV}{fm^3}$)	2.24

cavitation starts earlier for increasing the chemical potential.

TABLE III: Time when cavitation starts (in Fig. 4(a))

$\tau_{cav} [fm]$ (fixed $T_{initial} = 305 MeV$)	
<i>Model 2</i> ($\mu = 50 MeV$)	2.91
<i>Model 2</i> ($\mu = 250 MeV$)	2.84
<i>Model 2</i> ($\mu = 500 MeV$)	2.63
<i>Model 3</i> ($\mu = 50 MeV$)	1.61
<i>Model 3</i> ($\mu = 250 MeV$)	1.41

TABLE IV: Time when cavitation starts (in Fig. 4(b))

$\tau_{cav} [fm]$ (fixed $\varepsilon_{initial} = 16 GeV/fm^3$)	
<i>Model 2</i> ($\mu = 50 MeV$)	4.04
<i>Model 2</i> ($\mu = 250 MeV$)	3.8
<i>Model 2</i> ($\mu = 500 MeV$)	3.15
<i>Model 3</i> ($\mu = 50 MeV$)	2.18
<i>Model 3</i> ($\mu = 250 MeV$)	1.43

IV. CAVITATION IN A NON-CONFORMAL HOLOGRAPHIC PLASMA

One interesting question is whether it is possible to find cavitation within different approaches for the underlying many-body microscopic dynamics. From the strongly coupled

nature of the QGP, in particular near the deconfinement transition temperature, the microscopic physics should be inherently non-perturbative. In this context, holographic methods may shed light upon the nature of transport coefficients for such strongly coupled plasmas, since these coefficients are difficult to obtain from lattice methods.

We follow the parametrization and second-order theory from [16]. Considering Bjorken symmetry and flat spacetime, our analysis reduces to solving the following dissipative equations:

$$\tau_{\Pi}^{\eta} \left(D\pi^{\langle\mu\nu\rangle} + \frac{4\theta}{3}\pi^{\mu\nu} \right) + \pi^{\mu\nu} = -2\eta\sigma^{\mu\nu} + \frac{\lambda_1}{\eta^2}\pi_{\lambda}^{\langle\mu}\pi^{\nu\rangle\lambda} + \tau_{\pi}^*\pi^{\mu\nu}\frac{\Pi}{3\zeta} \quad (30)$$

and

$$\tau_{\Pi}^{\zeta} (D\Pi + \Pi\theta) + \Pi = -\zeta\theta + \frac{\xi_1}{\eta^2}\pi_{\mu\nu}\pi^{\mu\nu} + \frac{\xi_2}{\zeta^2}\Pi^2 + \tau_{\Pi}^{\zeta}\Pi D \ln \left(\frac{\zeta}{s} \right). \quad (31)$$

The employed holographic method is a bottom-up solution [33] that parametrizes some of the thermodynamical properties of lattice (2+1)-flavor QCD near the crossover phase transition, described by *Model 2* at zero chemical potential with the parameters given in [34]: $h_0 = 0.1396$, $h_1 = -0.1800$, $h_2 = 0.0350$, $f_0 = 2.76$, $f_1 = 6.79$, $f_2 = -5.29$, $g_1 = -0.47$ and $g_2 = 1.04$ as in [16]. It is known that holographic calculations of transport coefficients, such as the holographic value of $\eta/s = 1/4\pi$ [23], are generally consistent with experimental investigations of the evolution of QGP. The calculations employing usual kinetic theory result in larger values of η/s , which corroborates that holographic calculations are at least consistent with the QGP evolution near the deconfinement region [35].

The advantage of this approach is that the non-trivial temperature dependence of the transport coefficients were calculated for a phenomenological bottom-up model and parametrized in [16]. In the next subsection we summarize the relevant results.

A. Transport coefficients and Bjorken flow

The coefficient η/s is still $1/4\pi$, as is expected for several holographic models [23, 36]. The shear relaxation time is parametrized as follows ($T_c^h = 143.8$ MeV):

$$\frac{\tau_{\Pi}^{\eta}}{T^2} \eta \left(x = \frac{T}{T_c^h} \right) = \frac{a_{\eta}^h}{1 + e^{b_{\eta}^h(c_{\eta}^h - x)} + e^{d_{\eta}^h(e_{\eta}^h - x)} + e^{f_{\eta}^h(g_{\eta}^h - x)}}, \quad (32)$$

where a_{η}^h to g_{η}^h are fit parameters listed in Tab. V.

The parametrization of bulk viscosity is:

$$\frac{\zeta}{s} \left(x = \frac{T}{T_c^h} \right) = \frac{a_{bulk}^h}{\sqrt{(x - b_{bulk}^h)^2 + (c_{bulk}^h)^2}} + \frac{d_{bulk}^h}{x^2 + (e_{bulk}^h)^2}, \quad (33)$$

where a_{bulk}^h to e_{bulk}^h are fit parameters in Tab. V.

In order to parametrize the bulk relaxation time, we adopt a causality bound, relating it to the shear relaxation time [16]:

$$\tau_{\Pi}^{\zeta} T \left(x = \frac{T}{T_c^h} \right) = \frac{a_{\zeta}^h}{\sqrt{(x - b_{\zeta}^h)^2 + (c_{\zeta}^h)^2}} + \frac{d_{\zeta}^h}{x}, \quad (34)$$

with the corresponding fit parameters a_{ζ}^h to d_{ζ}^h being given in Tab. V.

TABLE V: Parameters: $\tau_{\Pi}^{\eta} \eta/T^2$ for Eq. (32), ζ/s for Eq. (33) and $\tau_{\Pi}^{\zeta} T$ for Eq. (34).

a_{η}^h	b_{η}^h	c_{η}^h	d_{η}^h	e_{η}^h	f_{η}^h	g_{η}^h
0.2664	2.029	0.7413	0.1717	-10.76	9.763	1.074
a_{bulk}^h	b_{bulk}^h	c_{bulk}^h	d_{bulk}^h	e_{bulk}^h		
0.01162	1.104	0.2387	-0.1081	4.870		
a_{ζ}^h	b_{ζ}^h	c_{ζ}^h	d_{ζ}^h			
0.05298	1.131	0.3958	-0.05060			

The other coefficients are determined in a phenomenological approach. However there is still a non-trivial behavior near the transition temperature. These are estimates considering fluid-gravity calculations for conformal fluid, as well as other strongly coupled holographic calculations [24, 37, 38]. We consider then the following [16]:

$$\begin{aligned} \lambda_1 &= \frac{2\eta^2}{sT}, \\ \tau_{\pi}^* &= -3\tau_{\Pi}^{\eta} \left(\frac{1}{3} - c_s^2 \right), \\ \xi_1 &= \lambda_1 \left(\frac{1}{3} - c_s^2 \right), \\ \xi_2 &= 2\eta\tau_{\Pi}^{\zeta} c_s^2 \left(\frac{1}{3} - c_s^2 \right). \end{aligned} \quad (35)$$

It is straightforward to solve Eqs. (30) and (31) in the Bjorken flow. We follow the conventions adopted in the previous section, so the evolution equations are (15) and the following:

$$\tau_{\Pi}^{\eta} \frac{\partial \Phi}{\partial \tau} = \frac{4\eta}{3\tau} - \Phi - \left[\frac{4\tau_{\Pi}^{\eta}}{3\tau} \Phi + \frac{\lambda_1}{2\eta^2} \Phi^2 \right] + \frac{\tau_{\pi}^*}{3\zeta} \Phi \Pi \quad (36)$$

and

$$\tau_{\Pi}^{\zeta} \frac{\partial \Pi}{\partial \tau} + \tau_{\Pi}^{\zeta} \frac{\Pi}{\tau} = -\frac{\zeta}{\tau} - \Pi + \frac{3}{2} \frac{\xi_1}{\eta^2} \Phi^2 + \frac{\xi_2}{\zeta^2} \Pi^2 + \frac{\tau_{\Pi}^{\zeta}}{(\zeta/s)} \left[\frac{\partial}{\partial T} \left(\frac{\zeta}{s} \right) \right] \frac{\partial T}{\partial \tau}. \quad (37)$$

In particular, equations (36) and (37) are the same as (16) and (17) but with extra transport coefficients. One interesting feature of such second order theory is that both bulk and shear evolution equations are nonlinear and coupled to each other. The entropy density in (33), (36) and (37) is calculated via (11).

We solve numerically Eqs. (15), (36) and (37) in the Bjorken flow and with the discussed holographic transport coefficients to search possible indications of cavitation. We consider the initial conditions $\tau_0 = 0.5 \text{ fm}$, $\Phi(\tau_0) = 0$, $\Pi(\tau_0) = 0$ for both initial approaches $T_{initial} = 305 \text{ MeV}$ and also $\varepsilon_{initial} = 16 \text{ GeV}/\text{fm}^3$.

As can be seen in Fig. 5 cavitation does not occur. It is often the case with holographic transport coefficients that dissipative effects seem to be smaller than others obtained from different methods, such as kinetic theory calculations. Nonetheless, the holographic values for small ratio of shear viscosity per entropy density are consistent so far with experimental results, and thus we suggest that, if confirmed by experimental data, the absence of cavitation may be a consequence of the strongly coupled nature of QGP.

V. CONCLUSIONS

In this work, we considered several equations of state at different chemical potentials in order to investigate the occurrence of cavitation in QGP. This was done through a numerical integration of the Bjorken hydrodynamical equations and determination of the pressure as a function of proper time.

We used a phenomenological parametrization of the lattice QCD equation of state for two sets of transport coefficients. For the bulk viscosity we used a parametrization of results obtained in a Monte-Carlo simulation of pure gluodynamics SU(3) [11, 39]. For both lattice QCD and mean field QCD equations of state, cavitation occurs at smaller time scales as

the chemical potential increases. In particular, the $(g/m_g)^2$ term in (26) enhances the finite chemical potential contribution. The cooling process is faster for larger chemical potentials.

As is often the case with transport coefficients calculated with lattice methods near phase transition, the height of the bulk per entropy density peak is not generally well established and most calculations rely on pure glue dynamics and consequently first order phase transitions. We considered a phenomenological holographic calculation of transport coefficients of a non-conformal QGP [16]. In our approach, we concluded that cavitation does not occur in the holographic prescription. This suggests that even the addition of more transport coefficients, which contain peaks near the crossover phase transition, does not support cavitation. In the future it may be possible to compare these distinct cavitation results in the scenario where lattice calculations of bulk effects can consistently consider the crossover phase transition.

It should be interesting to generalize our calculations to more complex flows and check whether cavitation can be obtained in different regimes.

Acknowledgments

This work was partially financed by the Brazilian funding agencies CAPES, CNPq and FAPESP. We thank J. Noronha and G. Torrieri for instructive discussions.

-
- [1] K. Adcox *et al.* [PHENIX Collaboration], Nucl. Phys. A **757**, 184 (2005)
 - [2] J. Adams *et al.* [STAR Collaboration], Phys. Rev. Lett. **91**, 172302 (2003)
 - [3] K. Aamodt *et al.* [ALICE Collaboration], Phys. Rev. Lett. **105**, 252301 (2010)
 - [4] B. Muller, J. Schukraft and B. Wyslouch, Ann. Rev. Nucl. Part. Sci. **62**, 361 (2012).
 - [5] P. Romatschke, Int. J. Mod. Phys. E **19**, 1 (2010).
 - [6] U. Heinz and R. Snellings, Ann. Rev. Nucl. Part. Sci. **63**, 123 (2013).
 - [7] T. Schaefer and D. Teaney, Rept. Prog. Phys. **72**, 126001 (2009).
 - [8] C. Gale, S. Jeon, B. Schenke, P. Tribedy and R. Venugopalan, Phys. Rev. Lett. **110**, 012302 (2013).
 - [9] G. Torrieri, B. Tomasik and I. Mishustin, Phys. Rev. C **77**, 034903 (2008).

- [10] G. Torrieri and I. Mishustin, *Phys. Rev. C* **78**, 021901 (2008).
- [11] K. Rajagopal and N. Tripuraneni, *JHEP* **1003**, 018 (2010).
- [12] A. Andronic, *Int. J. Mod. Phys. A* **29**, 1430047 (2014).
- [13] A. Dumitru, L. Portugal and D. Zschesche, *Phys. Rev. C* **73**, 024902 (2006).
- [14] S. Borsanyi, G. Endrodi, Z. Fodor, S. D. Katz, S. Krieg, C. Ratti and K. K. Szabo, *JHEP* **1208**, 053 (2012); Y. Aoki, G. Endrodi, Z. Fodor, S. D. Katz and K. K. Szabo, *Nature* **443**, 675 (2006).
- [15] S. Borsanyi, Z. Fodor, C. Hoelbling, S. D. Katz, S. Krieg and K. K. Szabo, *Phys. Lett. B* **730**, 99 (2014).
- [16] S. I. Finazzo, R. Rougemont, H. Marrochio and J. Noronha, *JHEP* **1502**, 051 (2015).
- [17] M. Habich and P. Romatschke, *JHEP* **1412**, 054 (2014).
- [18] G. S. Denicol, C. Gale and S. Jeon, arXiv:1503.00531 [nucl-th].
- [19] D. A. Fogaça, H. Marrochio, F. S. Navarra and J. Noronha, *Nucl. Phys. A* **934**, 18 (2014).
- [20] W. Israel, *Annals Phys.* **100**, 310 (1976); W. Israel and J. M. Stewart, *Annals Phys.* **118**, 341 (1979).
- [21] J. D. Bjorken, *Phys. Rev. D* **27**, 140 (1983).
- [22] A. Muronga, *Phys. Rev. C* **69**, 034903 (2004).
- [23] P. Kovtun, D. T. Son and A. O. Starinets, *Phys. Rev. Lett.* **94**, 111601 (2005).
- [24] R. Baier, P. Romatschke, D. T. Son, A. O. Starinets and M. A. Stephanov, *JHEP* **04** (2008) 100.
- [25] A. Bazavov *et al.*, *Phys. Rev. D* **80**, 014504 (2009).
- [26] S. M. Sanches, F. S. Navarra and D. A. Fogaça, *Nucl. Phys. A* **937**, 1 (2015).
- [27] D. A. Fogaça and F. S. Navarra, *Phys. Lett. B* **700**, 236 (2011).
- [28] B. Franzon, D. A. Fogaça, F. S. Navarra and J. E. Horvath, *Phys. Rev. D* **86**, 065031 (2012).
- [29] R. J. Furnstahl and Brian D. Serot, *Phys. Rev. C* **41**, 262 (1990).
- [30] R. F. Tooper, *Astrophys. J.* **156**, 1075 (1969).
- [31] A. Chodos, R. L. Jaffe, K. Johnson, C. B. Thorn and V. F. Weisskopf, *Phys. Rev. D* **9**, 3471 (1974).
- [32] D. A. Fogaça, L. G. Ferreira Filho and F. S. Navarra, *Phys. Rev. C* **81**, 055211 (2010).
- [33] S. S. Gubser and A. Nellore, *Phys. Rev. D* **78**, 086007 (2008).
- [34] Sz. Borsanyi, G. Endrodi, Z. Fodor, S. D. Katz, S. Krieg, C. Ratti and K. K. Szabo, *JHEP*

08 (2012) 053.

- [35] G. S. Denicol, T. Koide and D. H. Rischke, Phys. Rev. Lett. **105**, 162501 (2010); G. S. Denicol, J. Noronha, H. Niemi and D. H. Rischke, Phys. Rev. D **83**, 074019 (2011); G. S. Denicol, H. Niemi, E. Molnar and D. H. Rischke, Phys. Rev. D **85**, 114047 (2012).
- [36] A. Buchel and J. T. Liu, Phys. Rev. Lett. **93**, 090602 (2004).
- [37] S. Bhattacharyya, V. E. Hubeny, S. Minwalla and M. Rangamani, JHEP **0802**, 045 (2008).
- [38] I. Kanitscheider and K. Skenderis, JHEP **0904**, 062 (2009).
- [39] H. B. Meyer, Phys. Rev. Lett. **100**, 162001 (2008).
- [40] A. Jaiswal, R. S. Bhalerao and S. Pal, Phys. Rev. C **87**, 021901 (2013).

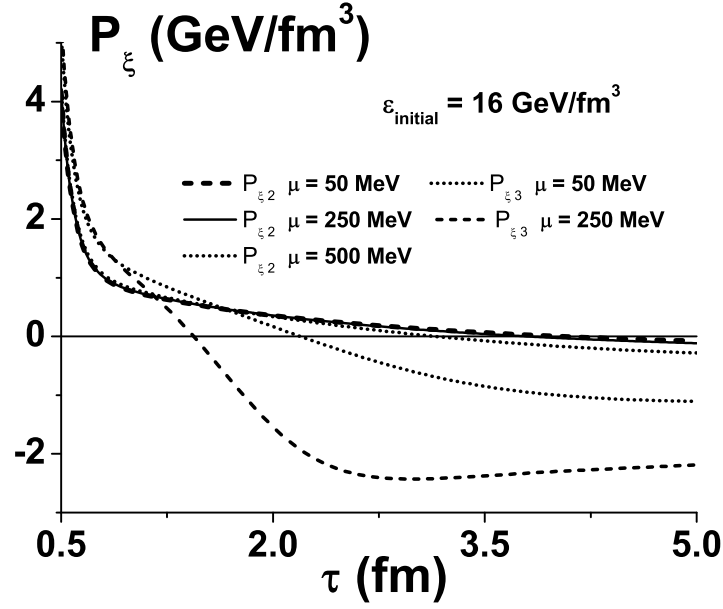
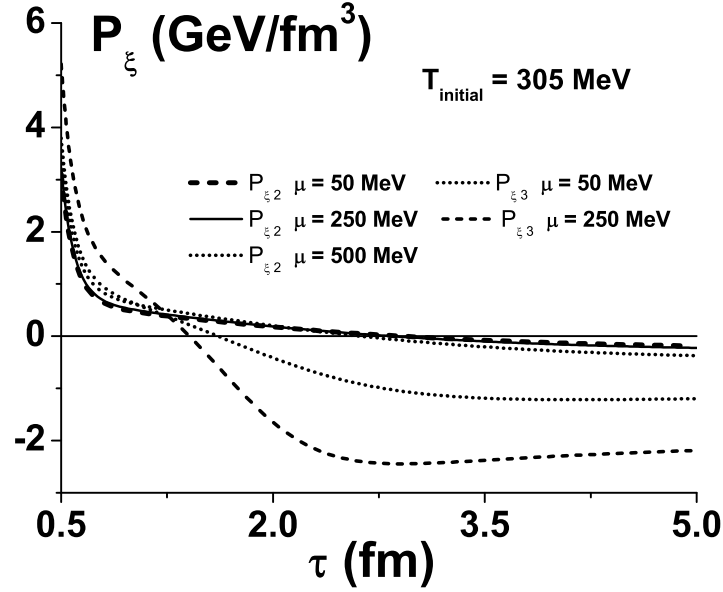
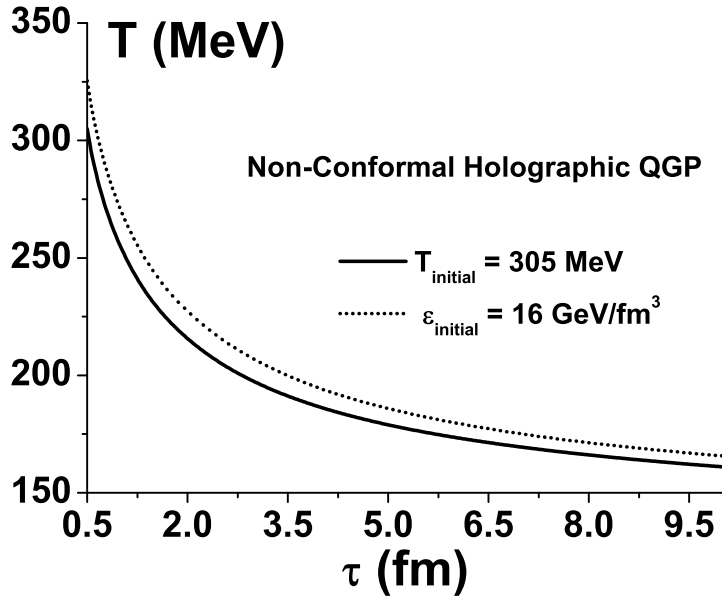
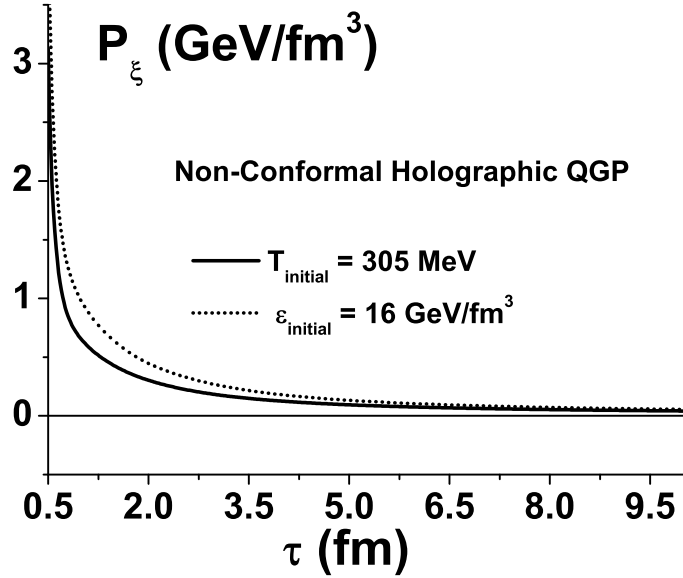


FIG. 4: Time evolution of the longitudinal pressure (14) from $\tau_0 = 0.5 \text{ fm}$ and finite chemical potential. (a) *Model 2*. (b) *Model 3* with $B_{QCD} = 150 \text{ MeV/fm}^3$, $g = 0.6$ and $m_g = 200 \text{ MeV}$. See Tables III and IV for values of the chemical potential. a) Same initial temperature. b) Same initial energy density.



(a)



(b)

FIG. 5: (a) Temperature evolution for the non-conformal holographic QGP. (b) Time evolution of the longitudinal pressure (14) for the non-conformal holographic QGP at zero chemical potential.